Journal of Materials Chemistry A

Accepted Manuscript

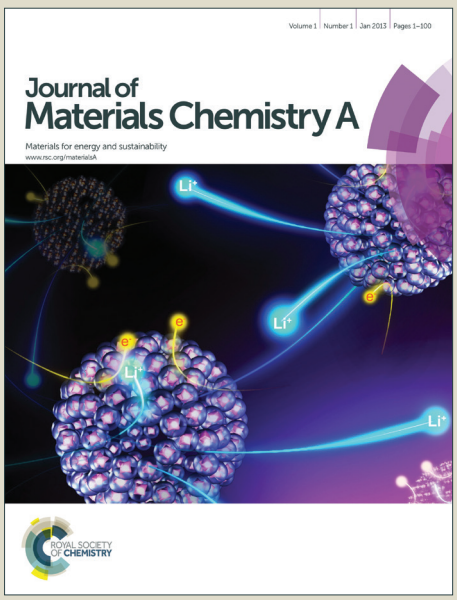

ROYAL SOCIETY OF CHEMISTRY

www.rsc.org/materialsA

Graphical abstract

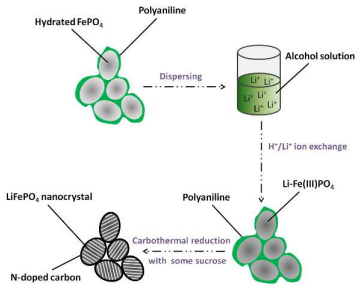

The paper reports a novel and universal lithiation of amorphous hydrated $FePO_4$, typically nanoscale $FePO_4$/polyaniline composite, by a facile H^+/Li^+ ion exchange reaction for fabricating $LiFePO_4$/C nanomaterial with high performances.

Cite this: DOI: 10.1039/c0xx00000x

www.rsc.org/xxxxxx

ARTICLE TYPE

Design and synthesis of high performance $LiFePO_4$/C nanomaterial for lithium ion batteries assisted by a facile H^+/Li^+ ion exchange

Hongbin Wang,[a] Lijia Liu,[a] Runwei Wang,[a] Daliang Zhang,[a] Liangkui Zhu,[a] Shilun Qiu,[a] Yingjin Wei,[b] Xu Jin,[c] and Zongtao Zhang[a,b,*]

Received (in XXX, XXX) Xth XXXXXXXXX 20XX, Accepted Xth XXXXXXXXX 20XX
DOI: 10.1039/b000000x

The main objective of this work is to find out a novel and universal lithiation of amorphous hydrated $FePO_4$, typically nanoscale $FePO_4$/polyaniline composite, by a facile H^+/Li^+ ion exchange reaction proceeding in nonaqueous medium that was attentively deduced and studied with the help of several chemical/physical analytical techniques. The resulting Li-derivative is proved to be a desirable precursor for fabricating $LiFePO_4$/C nanomaterial with ideal structural features containing highly crystalline $LiFePO_4$ nanoparticles completely coated with N-doped conductive carbon. More importantly, the $LiFePO_4$/C nanomaterial is capable of offering excellent rate capability and appealing cyclability that was strongly supported by the results of cyclic voltammogram (CV) and electrochemical impedance spectroscopy (EIS) tests.

Introduction

Rechargeable lithium ion batteries (LIBs) with the advantageous features of high operating voltage, superior energy density, long cycling life and no memory effect have gradually conquered the portable electronics market.[1,2] However, their implementations into electric transportation such as hybrid electric vehicles (HEVs) and electric vehicles (EVs) are constantly postponed in view of the performance, cost, environmental compatibility and particularly, safety concerns.[3,4] Olivine-type lithium ion phosphate ($LiFePO_4$), one of the very popular positive electrode materials for LIBs, is naturally abundant and thermodynamically stable, which has been proposed as a promising substitute for the high-priced and toxic cobalt-involved cathode materials that are still adopted by the vast majority of commercial LIBs so far.[5-7] Despite sluggish kinetics imposed by inherently poor electronic as well as ionic conductivity, desired capabilities turn out to be available for $LiFePO_4$ by synergetic effect of size tailoring in conjunction with conductive surface modification, typically with carbon materials.[8-10] To this end, multifarious strategies with respect to research and development of $LiFePO_4$/C nanomaterials emerge successively,[11,12] in which $FePO_4$-based synthetic route is widely approved.[13-15] Commonly used lithiation of $FePO_4$ basically relies on high temperature solid-state reaction that often entails tedious grinding (or ball milling) and long-time calcining cycles, thus leading to too much energy and time consumption.[13] On this account, some researchers have turned their attention to developing milder lithiation strategies by using low-temperature soft chemical synthesis technologies under atmospheric pressure, which in principle enables all the elemental components to distribute homogeneously at the atomic scale yet with little morphologies deterioration, thus facilitating the following fabrication of high-qualitied $LiFePO_4$/C nanomaterials in a more facile way.[16] Regrettably, to the best of our knowledge, all the successful attempts to date are reductant based (e. g. LiI or ascorbic acid).[17,18] Thus finding more reasonable synthetic schemes would be of great interest.

It is well established that the structure of hydrated $FePO_4$ (e. g. $FePO_4 \cdot 2H_2O$) consists of FeO_5OH_2 octahedra corner shared through PO_4 tetrahedra, leading to a three dimensional network with tunnels running along the b axis and occupied by the hydrogen atoms.[19] The possible mobility of protons belonging to the –OH and/or $–OH_2$ groups of hydrated compound, under appropriate conditions, may favor exchanges by Li^+ ions, as previously reported about $VO(HPO_4) \cdot H_2O$ or $FePO_4 \cdot H_2O$.[20,21] Supposing that the structure of hydrated compound is lack of long-range order, there potentially expose much more accessible –OH and/or $–OH_2$ groups for Li^+ ions to exchange with. On the basis of these hypotheses, we think that it may be achievable for lithiation of nano-sized amorphous hydrated $FePO_4$ through a simplex H^+/Li^+ ion exchange process, and afterwards yielding $LiFePO_4$/C nanomaterial by a carbothermal reduction reaction.

Experimental

Synthesis

$FePO_4$/polyaniline ($FePO_4$-PANI) nanocomposite was prepared by an in situ polymerization restriction method. Typically, 300 mL of aqueous solution containing 18.5 g $FeCl_3 \cdot 6H_2O$ was

slowly added, with vigorous stirring, to 600 ml of aqueous solution containing 7.86 g $NH_4H_2PO_4$ and 3 mL aniline. The suspension was then further stirred for 5 h at room temperature (~25 ℃). The resulting green precipitate was collected by filtration and washed several times with deionized water before being dried at 60 ℃ for 24 h.

Li-$FePO_4$/polyaniline (Li-$FePO_4$-PANI) was obtained through a facile chemical lithiation procedure that proceeded in a nonaqueous medium. In a typical run, 2.325 g of as-prepared $FePO_4$-PANI was firstly dispersed in 60 mL of 0.6 M lithium acetate alcohol solution. The reaction system was then raised to 60 ℃ and kept for 2 h. After cooling down naturally, the obtained grey-green precipitate was filtered, and dried at 60 ℃ for 2 h.

$LiFePO_4$/C nanomaterial was synthesized from Li-$FePO_4$-PANI intermediate by mixing it with sucrose under the mass ratio of 5:1. The mixture was finally transferred into a tube furnace and sintered at 700 ℃ for 6 h under an Ar atmosphere.

Characterizations

X-ray diffraction (XRD) patterns were recorded on a Rigaku D/MAX-2550 diffractometer at 50 kV and 200 mA with Cu Ka radiation **(**λ=1.5418 Å**)**. Fourier transform infrared spectrometer (FTIR) spectra were tested by a Bruker IFS-66V/S spectrometer. X-ray photoelectron spectroscope (XPS) measurements were performed on an ESCA LAB MARK Ⅱ spectrometer. Thermogravimetry-differential thermal analysis (TG-DTA) tests were conducted on a Netzsch STA 449C analyzer in air from room temperature to 700 ℃ at a heating rate of 10 ℃ min^{-1}. Nitrogen absorption-desorption isotherms were evaluated on a Micromeritics ASAP 2020M instrument. The specific surface areas were calculated employing the Brunauer-Emmett-Teller (BET) equation, and pore size distributions were obtained by Barrett-Joyner-Halenda (BJH) model. Morphology details were examined by JEOL JSM-6700F scanning electron microscope (SEM) and JEOL JSM-3010 transmission electron microscopy (TEM). CHN analysis of $LiFePO_4$/C composite was carried out by an Elementer Vario MICRO cube analyzer. Raman spectrum was collected with a Renishaw inVia Raman microscope and fitted using Gaussian model.

Electrochemical tests

For the electrochemical test, 80 wt. % of active material, 12 wt. % of acetylene black (AB) and 8 wt. % of polyvinylidene fluoride (PVDF) were firstly mixed evenly with N-methyl-2-pyrrolidinone (NMP). The obtained blended slurry was then casted on an aluminum foil current collector. After being dried thoroughly in vacuum, the electrode sheet was tailored into disks of Φ10 mm and assembled in CR2032 coin-type cells with lithium metal as counter electrode in an Ar-filled glovebox. The loading mass of active material in the electrode is 1~2 mg (area of 0.785 cm^2). The mixed solution of ethylene carbonate (EC), ethylmethyl carbonate (EMC) and dimethyl carbonate (DMC) (1:1:1 by volume) containing 1 M $LiPF_6$ was used as electrolyte. Celgard 2400 microporous membrane served as separator. Galvanostatic charge-discharge measurements were carried out in the voltage window of 2.0-4.3 V (vs. Li/Li^+) using a battery test system (CT2001A, Land). Cyclic voltammetry (CV) and electrochemical impedance spectroscopy (EIS) were measured on a Bio-Logic VSP electrochemical workstation. CV curves were recorded with increasing scanning rates from 0.5 to 10 mV s^{-1} (2.0-4.3 V). EIS was collected at open circuit voltage (OCV) after three cycles of activation in the frequency range of 200 KHz-10 mHz (amplitude of 5 mV). All the electrochemical tests were performed at ambient temperature (~25 ℃).

Results and discussion

To verify the above theoretical predictions, $FePO_4$/polyaniline ($FePO_4$-PANI) nanocomposite was firstly prepared by an in situ polymerization restriction method.[13] The process involves the addition of Fe^{3+} ions to a solution containing PO_4^{3-} ions and aniline that can be summarized as follows:

$$Fe^{3+}(aq) + PO_4^{3-}(aq) \longrightarrow FePO_4(s) \quad (1)$$

$$n\,(\text{Aniline}) \xrightarrow{Fe^{3+}} \text{Polyaniline}\,(s) \quad (2)$$

Here, Fe^{3+} ion acts as both a precipitator for PO_4^{3-} and oxidant for aniline. After being dispersed in a lithium acetate alcohol solution and stirred for 2 h, this $FePO_4$-PANI composite gradually evolves into an amorphous Li-derivative (Li-$FePO_4$-PANI) that has been proved to be an ideal precursor of high-qualitied $LiFePO_4$/C nanomaterial. The synthetic procedure can be schematically described as Figure 1, and detailed information will be given in the following sections. As suggested by XRD and FTIR analysis (Figure 2A and 2B), $FePO_4$-PANI composite is totally amorphous wherein small amounts of polyaniline are detectable, in good agreement with the previous report.[13] According to the calculative results of time-consumed test (expatiated in Supporting Information Figure S1), the chemical formula of hydrated $FePO_4$ part should be accurately described as $FePO_4$ $2.384H_2O$, and the mass fraction of polyaniline is about 4.47 %.

By comparing the FTIR spectra of $FePO_4$-PANI and Li-$FePO_4$-PANI, we can draw conclusions that H^+/Li^+ ion exchange treatment lowers little quantity of polyaniline, whereas the incorporation of Li^+ ions exerts a certain impact on the inorganic framework of hydrated $FePO_4$. Typically, the weakening of characteristic peak around 3205 cm^{-1}, belonging to the stretching

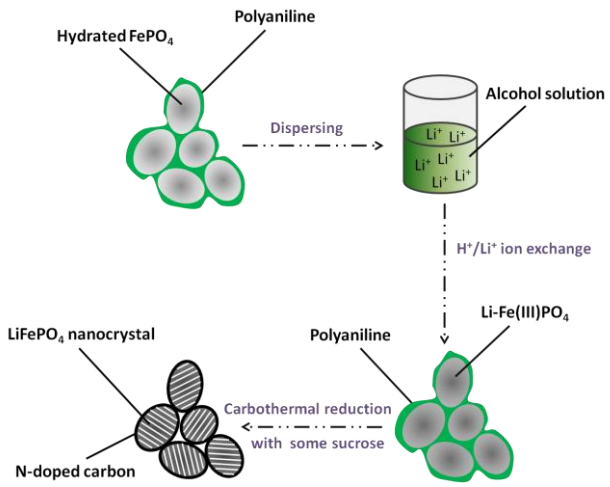

Figure 1. Schematic representation of proposed strategy for the synthesis of $LiFePO_4$/C nanomaterial assisted by a facile H^+/Li^+ ion exchange that proceeded in a nonaqueous medium.

Cite this: DOI: 10.1039/c0xx00000x

www.rsc.org/xxxxxx

ARTICLE TYPE

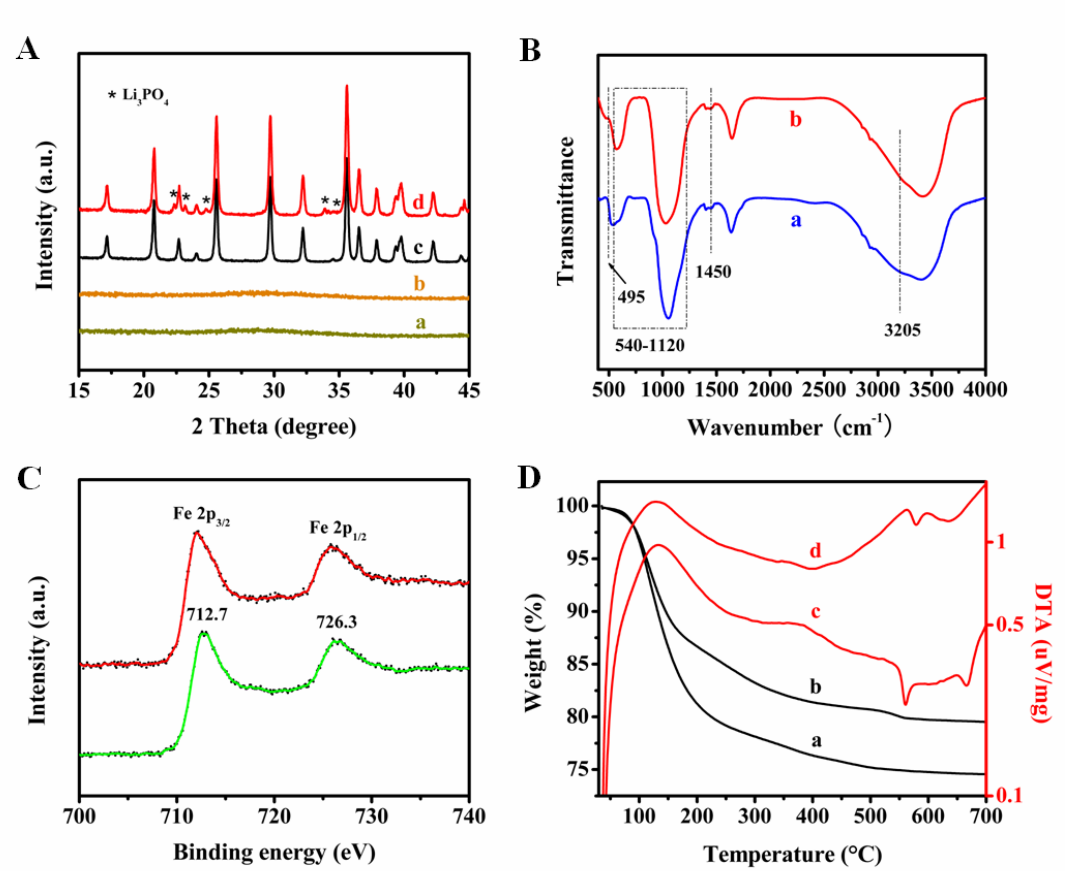

Figure 2. A) XRD patterns of a) $FePO_4$-PANI nanocomposite, b) Li-$FePO_4$-PANI nanocomposite, c) $LiFePO_4$/C nanomaterial achieved from Li-$FePO_4$-PANI and d) $LiFePO_4$/C material containing Li_3PO_4 impurity obtained from Li-excess intermediate. B) FTIR spectra of a) $FePO_4$-PANI and b) Li-$FePO_4$-PANI in the 400-4000 cm^{-1} region. The characteristic peak at 1450 cm^{-1} corresponds to benzene ring.[13] C) Fe 2p XPS curves of (green) $FePO_4$-PANI and (red) Li-$FePO_4$-PANI. D) TG curves of a) $FePO_4$-PANI and b) Li-$FePO_4$-PANI, DTA curves of c) $FePO_4$-PANI and d) Li-$FePO_4$-PANI.

vibration of O-H bond, should be attributed to the partial substitution of protons by Li^+ ions. This observation is well consistent with the appearance of a new band associated with the formation of Li-O unit at 495 cm^{-1}.[22-24] Theoretically, the presence of Li atoms linked to the bridging oxygen atoms in Li-$FePO_4$, instead of H ones in hydrated $FePO_4$, would partly destroy the intramolecular hydrogen bonds, thus leading to the strength of Fe-O bond (lessen the gap).[21] This variation of bond length could further spread to the entire framework and give rise to a slight structural distortion of phosphate anion. The above analysis may also help explain the phenomenon that the two composites take on distinguishing spectral curves in the wavenumber region of 540-1120 cm^{-1}.[25] XPS spectra, shown in Figure 2C, demonstrate that the two composites feature similar Fe 2p characteristic peaks, where binding energy values of Fe $2p_{3/2}$ and Fe $2p_{1/2}$ are both centered around 712.7 eV and 726.3 eV respectively, revealing that Fe species in $FePO_4$-PANI and Li-$FePO_4$-PANI are totally at iron (III) oxidation state.[26,27] Taken together, these results well support our initial theoretical prediction and explanation that the lithiation of $FePO_4$-PANI is just a cation exchange mechanism rather than complex redox behavior. The conclusion is further verified by the TG-DTA tests, as shown in Figure 2D. The total weight loss of Li-$FePO_4$-PANI is approximately 4.85 % lower than that of $FePO_4$-PANI, that is, close to the theoretical value of 4.93 %, confirming that almost one proton per hydrated $FePO_4$ formula unit has been replaced by Li^+. Detailed theoretical derivation is supplied in the supplementary information (Figure S1). Moreover, the major weight loss (or endothermic peaks) slightly shifts up towards the elevated temperature reign. This can be easily explained by the fact that the incorporation of Li^+ ions, partly breaking the "H_2O-like isolated molecules", makes the departure of H_2O component more difficult to occur, in good accordance with the analytical result of FTIR. Note that special care should be taken in

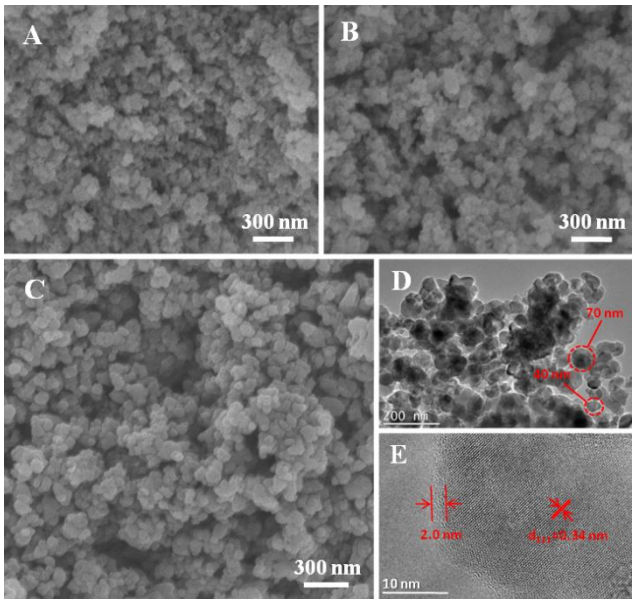

Figure 3. SEM images of A) $FePO_4$-PANI, B) Li-$FePO_4$-PANI and C) $LiFePO_4$/C nanomaterials. D) TEM image and E) high resolution TEM image of $LiFePO_4$/C nanomaterial.

controlling the exchanged amounts of Li^+ ion as excessive lithiating treatment (e. g. exchanging for 3 h) would give rise to the formation of crystalline Li_3PO_4 impurity in the final product (Figure 2Ad). It follows that the exchangeable protons belonging to the –OH and/or $–OH_2$ groups of $FePO_4$-PANI are more than one per hydrated $FePO_4$ formula unit, which may be related with the number of hydrated H_2O contained. Also worth a mention is the fact that controlled fabrication of $LiFePO_4$/C material turned out to be realizable as well when substituting pure hydrated $FePO_4$ (lack of PANI) for $FePO_4$-PANI composite (see Figure S2). The result firmly confirms that the H^+/Li^+ exchange process is mainly associated with hydrated $FePO_4$ rather than PANI polymer. In view of the simplex H^+/Li^+ ion exchange mechanism, it is believed that the synthetic scheme we proposed may be universal and could spread to lithiation of all sorts of amorphous hydrated $FePO_4$ that were widely reported over the past few years.[14,15]

Morphology analysis (Figure 3A and 3B) demonstrates that these two composites appear as similar porous agglomerate structures, and both of the primary particles are unable to distinguish clearly owing to the contribution of strongly cohesive effect induced by polyaniline polymer. The analogous observation is well supported by the results of N_2 adsorption-desorption characterization (Figure S3), which show almost identical textural parameters in terms of BET surface (39.9 vs. 39.8 $m^2\ g^{-1}$) and pore size distribution (inset in Figure S2). Based on this, we further consider that troublesome and destructive physical mixing step may be totally avoidable on the precondition that organic constituent (e. g. polymer) with sufficient amount has been in situ loaded on the outer surface of hydrated $FePO_4$ in advance. In this case, for one, the whole synthetic procedure would be greatly simplified; for the other, various morphologies rooting in local $FePO_4$-based precursors such as nanosheets, nanotubes, nanowires, hierarchical or hollow microspheres may be well preserved for the final $LiFePO_4$/C product that is very crucial for enhancing the electrochemical performances.

Subsequent heat treatment with some sucrose led to the conversion of this amorphous Li-$FePO_4$-PANI into highly crystalline $LiFePO_4$/C nanomaterial, as suggested by the XRD pattern (Figure 2Ac). All the reflections match well with the orthorhombic structure of olivine $LiFePO_4$ with no detectable impurity phase. The lack of carbon diffraction peaks is due to the amorphous structure characteristics coupled with lower content (6.03 wt. %). Morphology analysis clearly shows that $LiFePO_4$/C material consists of uniform nanoparticles (40-70 nm) that are connected together by surface carbon forming an aggregate structure (shown in Figure 3C). Such kind of agglomerating behaviour, almost inevitable for nano-sized $LiFePO_4$/C material during the calcining period at elevated temperature, will not issue in any negative influence on the batteries' properties. Usually, quite a few interspaces built by the accretion of the surrounding nanoparticles are still existent (see Figure 3D) that are sufficient to ensure the full penetration of electrolyte for the fast Li^+ ion transfer. On contrast, $LiFePO_4$/C material reasonably agglomerated by conductive carbon is supposed to greatly enhance the electrical continuity of entire electrode, and simultaneously facilitate the maneuverability in practice. High resolution TEM image, shown in Figure 3E, confirms that the $LiFePO_4$ particle is highly crystallined and covered by an amorphous carbon layer (~2.0 nm thickness). The detailed structural feature of the surface carbon was studied by Raman characterization (Figure 4). As fitted by Gaussian model, Raman spectrum can be exactly divided into four peaks, in which the peaks at 1356 cm^{-1} and 1588 cm^{-1} are assigned to D band (disordered carbon, sp^3) and G band (graphite, sp^2) of Raman vibration modes for amorphous carbon, respectively. The high peak intensity ratio I_G/I_D (~0.82) reflects that the residual carbon is more graphited, capable of providing good electric conductivity.[28] Besides, the lack of $LiFePO_4$ characteristic peaks in the wavenumber range of 600-1100 cm^{-1} illustrates that carbon coating on the surface of $LiFePO_4$ particles is fairly complete.[28] In view of one-dimensional Li^+ ion mobility in the framework, thoroughly surface-modified with carbon, could ensures $LiFePO_4$

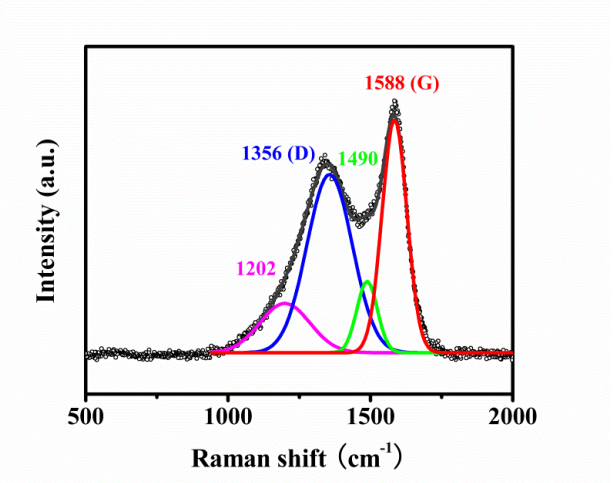

Figure 4. Raman spectrum of $LiFePO_4$/C nanomaterial fitted by Gaussian model.

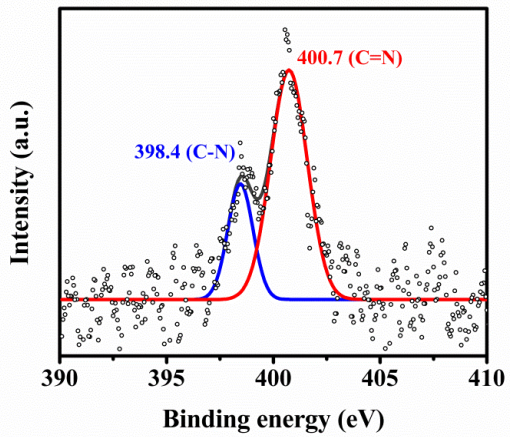

Figure 5. N 1s XPS spectrum of $LiFePO_4$/C nanomaterial fitted by Gaussian model.

particles get electrons from all directions, which ultimately alleviates electrode polarization.[13] It is noteworthy that nitrogen element in $LiFePO_4$/C composite was also detectable by XPS, as shown in Figure 5. The well-defined N 1s spectrum can be easily deconvoluted into two peaks at binding energies of 398.4 eV and 400.7 eV that were identified as C–N and C=N bonds respectively,[29] thus implying that the surface residual carbon derived from in situ carbonization of polyaniline mixed with sucrose is N-doped. Loosely speaking, C–N bonds generally locate at the interior of graphite sheets by direct substitution of C atoms with N ones, while C=N bonds appear at the edge and/or defect positions.[30] Despite trace amount (~1.53 wt. % of carbon matrix), the incorporation of nitrogen heteroatoms could produce large amounts of favorable defects in the carbon layer that indubitably would endow $LiFePO_4$/C nanomaterial with more enhanced surface electronic as well as ionic conductivity.[29,30]

Figure 6 shows cyclic voltammogram (CV) curves of $LiFePO_4$/C nanomaterial with various potential scan rates from

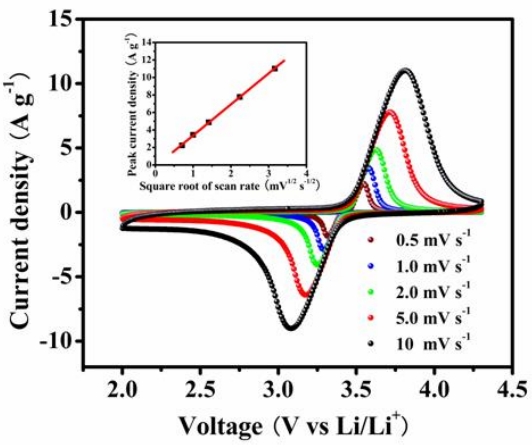

Figure 6. CV curves of $LiFePO_4$/C nanomaterial tested at various scan rates. Inset shows the linear fitting of peak current density versus square root of the scan rate.

0.5 mV s^{-1} up to 10 mV s^{-1}. All the CV curves are characterized by a couple of redox peak that corresponds to single Fe^{2+}/Fe^{3+} redox couple of orthorhombic $LiFePO_4$. Highly symmetric peak profiles indicate good reversibility of Li^+ ion extraction/insertion reactions. Even at a fast scan rate of 10 mV s^{-1}, symmetrical CV profile is also well reserved with no significant distortion. The result reflects a favorable electrochemical kinetics and allows us to expect an excellent rate capability. Besides that, the peak current density (typically during anodic scans) exhibits a linear relation with the square root of scanning rate (inset in Figure 6), typical diffusion controlling response, implying that the kinetics of two-phase transition in $LiFePO_4$/C behaves similar as a diffusion process.[31] For semi-infinite or finite diffusion, the linear relation can be used to extract the Li^+ diffusion coefficient (D_{Li+}) applying Randles-Sevcik equation:[32]

$$I_p=2.69\times10^5 n^{3/2} A D_{Li+}{}^{1/2} C v^{1/2}$$

where I_p is the peak current (A), n is the number of electrons per species reaction, A is the active surface area of electrode (cm^2), C is the shuttle concentration (mol cm^{-3}), and v is the scanning rate (V s^{-1}). According to the slope of the linear fit, the D_{Li+} of $LiFePO_4$/C material is calculated to be 1.226×10^{-10} cm^2 s^{-1}. It is found that the value is very close to that (the order of 10^{-11} cm^2 s^{-1}) reported by Liu et al.,[33] and much higher than the ones obtained by other groups.[34-36] Such fast ionic conductivity character, mostly ascribed to the well-crystalline olivine $LiFePO_4$ nanocrystals fully coated with thin and N-doped amorphous carbon, would favor high rate and hence high power applications.

The galvanostatic charge-discharge characteristics of $LiFePO_4$/C are shown in Figure 7A, 7B and S4. Expectedly, the material afforded an initial discharge capacity of 160.3 mAh g^{-1} at 0.2 C (1 C=170 mA g^{-1}), kept 137.1 mAh g^{-1} at 5 C, and also delivered a reversible capacity of 110.8 mAh g^{-1} at 30 C. Even the rates were up to 60 C and 100 C, discharge capacities could still reach as high as 95.2 mAh g^{-1} and 80.3 mAh g^{-1}, respectively. The result is much better than that of commercial $LiFePO_4$/C nanomaterial tested under otherwise identical conditions, and also superior to other reported ones that were achieved by various synthetic routes (Figure 7C). Typically, $LiFePO_4$/C nanomaterial synthesized by $FePO_4$-PANI based high temperature solid-state method can provide a discharging capacity of 80 mAh g^{-1} at a highest given rate of 60 C;[13] Ultrafine $LiFePO_4$ nanoparticles achieved by ascorbic acid assisted low temperature soft chemical lithiation method exhibit 100.7 mAh g^{-1} at 5C rate.[18] The fact that the particles of our $LiFePO_4$ material are nano-sized and fully surface-modified with N-doped conductive carbon is definitely in charge of its extreme rate capability, but the performance is substantially better than the result reported in other literature for particles of smaller size (20-40 nm),[13] indicating that the proposed H^+/Li^+ ion exchange also enhances the rate capability. After a series of varying rate tests, the reversible capacity almost recovered to the original value of ~160 mAh g^{-1} at 0.2 C, thus demonstrating the good structural stability of $LiFePO_4$/C nanomaterial under the large-current condition. The superior charge-discharge performance is well supported by the result of electrochemical impedance spectroscopy (EIS) measurement, as

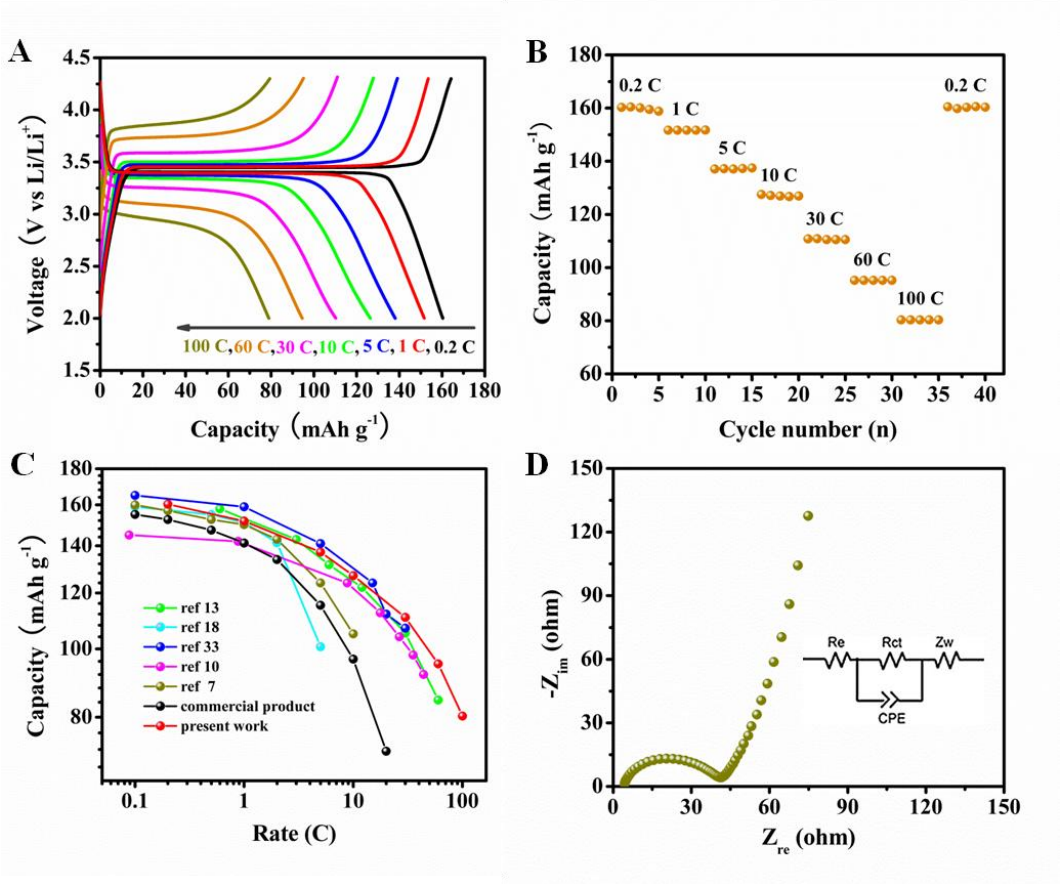

Figure 7. A) Galvanostatic charge-discharge curves of $LiFePO_4$/C nanomaterial tested at various rates. B) Discharge rate capability of $LiFePO_4$/C nanomaterial. C) Ragone plots of as-prepared and commercial $LiFePO_4$/C nanomaterials, together with those of other reported ones that were achieved by various synthetic routes: ref 13, $FePO_4$-PANI based high temperature solid-state method;[13] ref 18, ascorbic acid assisted low temperature soft chemical lithiation method;[18] ref 33, high-energy ball milling assisted high temperature solid-state method;[33] ref 10, coprecipitation method;[10] ref 7, microwave-solvothermal method.[7] D) Nyquist plots of $LiFePO_4$/C composite performed at open circuit voltage (OCV) after three cycles of activation. Inset in D) shows the equivalent circuit.

shown in Figure 7D. Typically, Nyquist plots are composed of a depressed semicircle in the high-to-medium frequency region together with a slope in the low frequency region. The former is mainly related with the charge transfer process, while the later is attributed to Warburg diffusion of Li^+ ions in the solid electrode. Besides, the high-frequency intercept at the real axis (Z_{re}) corresponds to the ohmic resistance (R_s) of the cell, which is driven by electrolyte, separator, electrode, contact, etc. The small high-frequency intercept coupled with a minor semicircle presages appealing interfacial charge kinetics.[37] On the basis of equivalent circuit given in the inset of Figure 7D, the fitted values of ohmic resistance and charge transfer resistance (R_{ct}) are determined to be 4 Ω and 39.2 Ω respectively, which are significantly lower than those (4.3 Ω and 93.5 Ω) of commercial $LiFePO_4$/C material (Figure S5). Of particular note is that our $LiFePO_4$/C nanomaterial can also exhibit a high discharging capacity of 84.7 mAh g^{-1} at 60 C rate when testing with a relatively higher mass loading of 5 mg cm^{-2}, as shown in Figure S6.

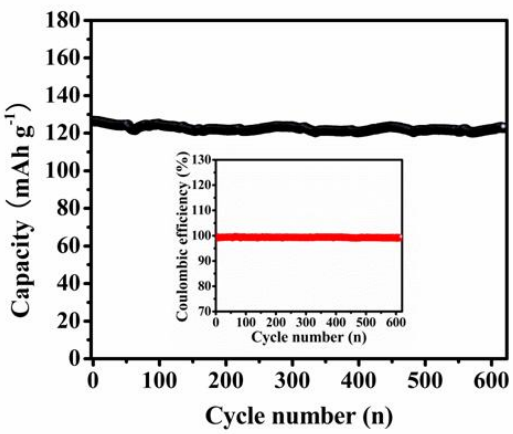

Figure 8. Long-term cycling performance of $LiFePO_4$/C nanomaterial evaluated at 10 C rate over 600 cycles. Inset shows corresponding coulombic efficiency.

Long-term cyclability was also studied by continuous charge-discharge test at a moderate rate of 10 C (Figure 8). In spite of nanoscale dimension, $LiFePO_4$/C material exhibits excellent capacity retention, with merely less than 3 % discharging capacity loss over 600 cycles, that is, equivalent of capacity decay ~0.005 % per cycle. During the cycling process, the coulombic efficiency based on the ratio of discharging capacity to charging one stays at nearly 100 % (inset in Figure 8).

Conclusions

In summary, we successfully developed a new strategy for the lithiation of amorphous hydrated $FePO_4$, typically $FePO_4$-PANI nanocomposite, by a facile H^+/Li^+ ion exchange reaction proceeding in nonaqueous medium that was attentively deduced and studied with the help of several chemical/physical analytical techniques. The resulting Li-derivative (Li-$FePO_4$-PANI) is proved to be a desirable precursor for fabricating $LiFePO_4$/C nanomaterial with ideal structural features containing highly crystalline $LiFePO_4$ nanoparticles completely coated with N-doped conductive carbon. More importantly, the $LiFePO_4$/C nanomaterial is capable of offering remarkable electrochemical performances in terms of rate capability and cyclability that was strongly supported by the results of CV and EIS tests. Also worth a mention is the fact that the H^+/Li^+ ion exchange procedure was found to be so mild that the particle morphology of initial $FePO_4$-PANI could be preserved almost perfectly for Li-$FePO_4$-PANI. It is thus conceivable that the proposed cation exchange technology in conjunction with proper polymer-riched hydrated $FePO_4$ may provide us an opportunity to realize facile and cost-effective fabrication of high-qualitied $LiFePO_4$/C nanomaterials beyond laboratory-scale limitations. Relevant studies are currently underway. We also hope that such a reasonable and controllable cation exchange approach would be extended to lithiation of various amorphous hydrated compounds, including but not limited to $FePO_4$, for LIBs applications or other else.

Acknowledgements

This work was supported by the National Natural Science Foundation of China (20841003 and 20741001), and the New Century Outstanding Scholar Supporting Program.

Notes and references

[a] *State Key Laboratory of Inorganic Synthesis and Preparative Chemistry, Jilin University, Changchun 130012, P. R. China*
E-mail: zzhang@jlu.edu.cn; Fax: +86-431-85168115; Tel: +86-431-85168115

[b] *Key Laboratory of Physics and Technology for Advanced Batteries (Ministry of Education), Jilin University, Changchun 130012, P. R. China*

[c] *Research Institute of Petroleum Exploration and Development, PetroChina, Beijing 100083, P. R. China*

† Electronic Supplementary Information (ESI) available: Time-consumed test, XRD patterns, N_2 adsorption-desorption characterization, charge and discharge curves, EIS measurement. See DOI: 10.1039/b000000x/

1 P. G. Bruce, B. Scrosati, J.-M. Tarascon, *Angew. Chem. Int. Ed.*, 2008, **47**, 2930-2946.
2 W.-B. Luo, S.-L. Chou, Y.-C. Zhai, H.-K. Liu, *J. Mater. Chem. A*, 2014, **2**, 4927-4931.
3 P. Gibot, M. Casas-Cabanas, L. Laffont, S. Levasseur, P. Carlach, S. Hamelet, J.-M. Tarascon, C. Masquelier, *Nat. Mater.*, 2008, **7**, 741-747.
4 H.-M. Xie, R.-S. Wang, J.-R. Ying, L.-Y. Zhang, A. F. Jalbout, H.-Y. Yu, G.-L. Yang, X.-M. Pan, Z.-M. Su, *Adv. Mater.*, 2006, **18**, 2609-2613.
5 M. K. Devaraju, I. Honma, *Adv. Energy Mater.*, 2012, **2**, 284-297.
6 C. Gong, F. Deng, C.-P. Tsui, Z. Xue, Y. S. Ye, C. Y. Tang. X. Zhou, X. Xie, *J. Mater. Chem. A*, 2014, **2**, 19315-19323.
7 A. V. Murugan, T. Muraliganth, A. Manthiram, *J. Phys. Chem. C*, 2008, **112**, 14665-14671.
8 J. Wang, X. Sun, *Energy Environ. Sci.*, 2012, **5**, 5163-5185.
9 X. Guo, Q. Fan, L. Yu, J. Liang, W. Ji, L. Peng, X. Guo, W. Ding, Y. Chen, *J. Mater. Chem. A*, 2013, **1**, 11534-11538.
10 M.-H. Lee, T.-H. Kim, Y. S. Kim, H.-K. Song, *J. Phys. Chem. C*, 2011, **115**, 12255-12259.
11 B. H. Rong, Y. W. Lu, X. W. Liu, Q. L. Chen, K. Tang, H. Z. Yang, X. Y. Wu, F. Shen, Y. B. Chen, Y. F. Tang, Y. F. Chen, *Nano Energy*, 2014, **6**, 173-179.
12 C. Sun, S. Rajasekhara, J. B. Goodenough, F. Zhou, *J. Am. Chem. Soc.*, 2011, **133**, 2132-2135.
13 Y. Wang, Y. Wang, E. Hosono, K. Wang, H. Zhou, *Angew. Chem. Int. Ed.*, 2008, **47**, 7461-7465.
14 X.-M. Liu, P. Yan, Y.-Y. Xie, H. Yang, X.-D. Shen, Z.-F. Ma, *Chem. Commun.*, 2013, **49**, 5396-5398.
15 R. R. Zhao, L. C. Zhu, Z. Z. Huang, J. Z. Liang, H. Y. Chen, *Ionics*, 2013, **19**, 581-588.
16 Y. Jiang, H. Zhuang, D. Pan, Z. Jiao, X. Que, X. Ling, M. Zhong, Y. Chu, B. Zhao, *J. Appl. Electrochem.*, 2013, **43**, 611-617.
17 P. P. Prosini, M. Carewska, S. Scaccia, P. Wisniewski, S. Passerini, M. Pasquali, *J. Electrochem. Soc.*, 2002, **149**, A886-A890.
18 B. Wang, Y. Qiu, S. Ni, *Solid State Ionics*, 2007, **178**, 843-847.
19 V. Pralong, V. Caignaert, B. Raveau, *J. Mater. Chem.*, 2011, **21**, 12188-12201.
20 D. Lozano-Calero, S. Bruque, M. A. G. Aranda, M. Marti-nez-Lara, L. Moreno, *J. Solid State Chem.*, 1993, **103**, 481-489.
21 N. Marx, L. Croguennec, D. Carlier, L. Bourgeois, P. Ku-biak, F. L. Cras, C. Delmas, *Chem. Mater.*, 2010, **22**, 1854-1861.
22 J. Santos-Peña, P. Soudan, C. O. Areán, G. T. Palomino, S. Franger, *J. Solid State Electrochem.*, 2006, **10**, 1-9.
23 R. Trócoli, J. Morales, J. S. Peña, *Solid State Ionics*, 2014, **255**, 30-38.
24 A. A. Salah, P. Jozwiak, K. Zaghib, J. Garbarczyk, F. Gen-dron, A. Mauger, C. M. Julien, *Spectrochimica Acta Part A*, 2006, **65**, 1007-1013.
25 K. Zaghib, C. M. Julien, *J. Power Sources*, 2005, **142**, 279-284.
26 C. Nan, J. Lu, L. Li, L. Li, Q. Peng, Y. Li, *Nano Res.*, 2013, **6**, 469-477.
27 L. Castro, R. Dedryvère, M. EI Khalifi, P.-E. Lippens, J. Bréger, C. Tessier, D. Gonbeau, *J. Phys. Chem. C*, 2010, **114**, 17995-18000.
28 J. Qian, M. Zhou, Y. Cao, X. Ai, H. Yang, *J. Phys. Chem. C*, 2010, **114**, 3477-3482.
29 L. Zhao, Y.-S. Hu, H. Li, Z. Wang, L. Chen, *Adv. Mater.*, 2011, **23**, 1385-1388.
30 Z. Ding, L. Zhao, L. Suo, Y. Jiao, S. Meng, Y.-S. Hu, Z. Wang, L. Chen, *Phys. Chem. Chem. Phys.*, 2011, **13**, 15127-15133.
31 K. Tang, X. Yu, J. Sun, H. Li, X. Huang, *Electrochimica Acta*, 2011, **56**, 4869-4875.
32 X. Yan, Y. Li, F. Du, K. Zhu, Y. Zhang, A. Su, G. Chen, Y. Wei, *Nanoscale*, 2014, **6**, 4108-4116.
33 W. L. Liu, J. P. Tu, Y. Q. Qiao, J. P. Zhou, S. J. Shi, X. L. Wang, C. D. Gu, *J. Power Sources*, 2011, **196**, 7728-7735.
34 Y. Zhao, L. Peng, B. Liu, G. Yu, *Nano Lett.*, 2014, **14**, 2849-2853.
35 N. Zhou, E. Uchaker, H.-Y. Wang, M. Zhang, S.-Q. Liu, Y.-N. Liu, X. Wu, G. Cao, H. Li, *RSC Adv.*, 2013, **3**, 19366-19374.
36 J. Du, L. Jiao, Q. Wu, Y. Liu, Z. Qi, L. Guo, Y. Wang, H. Yuan, *Electrochimica Acta*, 2013, **98**, 288-293.
37 J. Ni, M. Morishita, Y. Kawabe, M. Watada, N. Takeichi, T. Sakai, *J. Power Sources*, 2010, **195**, 2877-2882.